Transformation and structure of silicatelike CO_2-V

Choong-Shik Yoo,[1,*] Minseob Kim,[1] Wolfgang Morgenroth,[2] and Peter Liermann[3]
[1]*Department of Chemistry and Institute for Shock Physics, Washington State University, Pullman, Washington 99164, USA*
[2]*Institut für Geowissenschaften, Abt. Kristallographie, Goethe-Universität Frankfurt, D-60438 Frankfurt am Main, Germany*
[3]*Photon Sciences–PETRA III (FS-PE), Deutsches-Elektronen Synchrotron DESY, D-22603 Hamburg, Germany*
(Received 16 March 2013; published 17 June 2013)

We report the evidence of two different polymorphs for polymeric CO_2-V in tridymitelike (V_{TD} in $P2_12_12_1$) and β-cristobalitelike (V_{CR} in I-$42d$) structures. The V_{TD} phase is produced by laser-heating phase III (*Cmca*) above 40 GPa, whereas the V_{CR} phase by laser-heating highly compressed phase II ($P4_2/mnm$—iso-space group to stishovite) and IV ($P4_12_12$—iso-space group to α-cristobalite) above 35 GPa. The density of the V_{CR} (3.988 g/cm^3) is ~12% larger than that of the V_{TD} (3.559 g/cm^3) at 50 GPa, while the density difference reduces to ~4% at ambient pressure. This results in a substantially smaller bulk modulus ($B_o = 127$ GPa, $B' = 5.6$) for the V_{CR} phase than that of the V_{TD} ($B_o = 270$ GPa, $B' = 1.9$). The smaller density of the V_{TD} is due to the open structure of corner shared CO_4 tetrahedra and a great level of distortion in C-O-C angles resulting in a highly buckled layer structure; yet, the structural relationship gives rise to the specific transition to occur depending on the initial phase, either displacively from phase IV to phase V_{CR} or diffusively from phase III to phase V_{TD}. The results also provide new constraints for the phase/chemical transformation diagram of carbon dioxide.

DOI: 10.1103/PhysRevB.87.214103 PACS number(s): 81.40.Vw, 64.70.K−, 61.66.−f

I. INTRODUCTION

Carbon dioxide exhibits richness of high-pressure polymorphs with a great diversity in intermolecular interaction, chemical bonding, and crystal structures. It ranges from typical molecular solids (I, III, VII)[1,2] to intermediary phases (II, IV)[3–6] and to fully extended covalent solids with crystal structures similar to those of silicate minerals of pure silica (SiO_2). The silicalike extended solids have been reported at pressures above 40 to 70 GPa and temperatures of 300 to 2000 K. Those are fourfold CO_2-V,[7–12] sixfold CO_2-VI,[13,14] coesitelike CO_2 (c-CO_2),[15] and amorphous silicalike a-carbonia (a-CO_2).[16,17] These are fundamentally new materials, consisting of monolithic three-dimensional ($3D$) network structures of carbon atoms covalently bonded with oxygen atoms in CO_4 tetrahedra similar to those of silicate minerals (even in sixfold phase VI by means of disorder[13]). These solids exhibit low compressibility, strong optical nonlinearity, high energy density, high thermal conductivity, high phonon frequencies, and presumably high melting temperatures.[7,8] The large disparity in chemical bonding between the extended and molecular phases and relatively slow kinetics associated with the extended-to-molecular transitions, on the other hand, allow these extended solids to exist over a large pressure domain (down to a few GPa). At higher pressure-temperature conditions, these extended solids amorphize, ionize, and decompose.[18,19]

Phase V (CO_2-V) is the first discovered extended phase of carbon dioxide, produced by laser heating of phase III at ~40 GPa and ~1800 K.[7] The vibration spectrum of the quenched phase shows a strong COC stretch/bending mode at ~800 cm^{-1} at 40 GPa, clearly indicating that it is an extended covalent solid made of carbon-oxygen single bonds. The transition appears to have no strong dependence on temperature, indicating that the experimentally observed phase boundary is likely a kinetic barrier. In fact, the first principles calculation at 0 K suggests that such a molecular-to-nonmolecular phase transition would take place above 40 GPa.[8] The phase V can be quenched at ambient temperature as long as the pressure remains above 10 GPa. Below 10 GPa, it depolymerizes into phase I, although the remnant of polymeric phase V can be seen at substantially lower pressures down to 1 GPa where CO_2 liquidifies or sublimes.

Determining the crystal structure of phase V had been challenging for several reasons, including its coexistence with other phases due to an incomplete transformation of phase III and/or the metastability of other high temperature phases IV and II, the presence of large lattice distortion and highly preferred orientation. Nevertheless, the early x-ray diffraction data[9] indicated that the crystal structure was similar to that of tridymite ($P2_12_12_1$) in which each carbon atom is indeed tetrahedrally bound to four oxygen atoms in a corner-sharing tetrahedral configuration. We refer this phase to V_{TD} in short. Immediately after the x-ray study, first principles calculations however challenged the experimentally observed tridymite structure and predicted β-crystobalite to be the most stable structure among all fourfold candidates of silicate structures including α- and β-quartz, m-chalcopyrite, tridymite, and coesite.[8,10]

Recently, the crystal structure of phase V was reexamined using both pure and highly diluted CO_2 samples (1% CO_2 in He).[11] In these experiments, CO_2 samples were directly heated using a CO_2 laser, producing phase V without use of heat absorber. The structure was indeed found as a modified β-crystobalite structure (I-$42d$ or α-chalcopyrite).[11] We refer this later structure to phase V_{CR}. Interestingly, the V_{CR} phase is substantially denser (by ~12% at 40 GPa) but softer (less than half of B_o) than the V_{TD}. It also showed a great level of lattice distortion in the V_{CR} made from pure CO_2 samples but absent from highly diluted 1% CO_2 samples. Yet, the study has found no evidence for the presence of the tridymitelike V_{TD} phase reported earlier.[9]

Important to note, however, is that the collective behavior of carbon dioxide molecules in such a highly diluted condition (1% CO_2 in He)[11] can be greatly different from that of

pure CO_2. This includes the solubility between CO_2 and He, which can change significantly with pressure and especially temperature. Also, in the same study, pure CO_2 samples were initially heated at 21 GPa and ~1800 K to produce a mixture of phase II and IV. Then, the mixture was compressed to 39 GPa and laser heated to ~1800 K to produce the V_{CR}. Presumably, this was due to difficulty to directly heat CO_2-III by a CO_2 laser. In fact, another CO_2-laser-heating study[12] reported, "Non molecular CO_2 ... is easily heated once very small amount is formed, thereby providing a positive feedback to the laser-heating procedure." While this process can be easily understood in terms of flux crystallization using a small seed crystal,[12] it is not known if the initially formed crystal was phase IV (or II) or phase V_{CR}. In fact, these phases can be produced at relatively low temperatures below 400–500 °C (nearly on a touch of infrared heating laser)[3,5,6] and may have greatly different infrared absorption characteristics from phase III or I,[20] for example, as observed strong IR absorption in θ-N_2 and H_2-III phases.[21,22] Therefore, a relevant question to consider is if there is any path-dependence on the transition that can give rise to seemingly different results of these previous laser-heating experiments.[9,11,12]

Motivated by the above-mentioned diverse results of phase V, we have reexamined the crystal structure and transformation of carbon dioxide using spatially resolved x-ray diffraction with a small synchrotron x-ray beam (<2 μm) at the Positron-Electron Tandem Ring Accelerator (PETRA) III (Deutsches Elektronen-Synchrotron [DESY], Hamburg) and found both V_{TD} and V_{CR} present in the same sample. As such, the two phases are structurally related as in the case of SiO_2 polymorphs, and the transitions are indeed path dependent on the initial phases. The present result also shows that the V_{CR} is substantially denser and has a softer lattice compared to V_{TD}, resulting in the density difference within 5% at ambient condition.

II. EXPERIMENTS

Carbon dioxide samples were loaded into membrane-diamond-anvil cells from liquid by condensing CO_2 gas to −35 °C and 15 atmospheres. Type IA diamond anvils were used with a flat culet size of 0.3 mm. A rhenium gasket was preindented to 0.04–0.05 mm thick, and a small hole of ~0.12 mm was drilled using an electric-discharge microdrilling machine. A small piece of carbon (~0.01 mm in diameter and 0.05 mm long) was placed in the sample chamber to absorb the CW Nd: YLF laser ($\lambda = 1054$ nm) light and heat CO_2 samples. The sample pressure was measured using the Ruby luminescence method.[23] Existences and transitions of different carbon dioxide phases were *in situ* determined by x-ray diffraction and later confirmed by the characteristic Raman spectra of different phases.[3–5,7]

Here, CO_2-V was produced by laser heating CO_2-III above 40 GPa, which typically resulted in preferably oriented crystals or grains apparent from the sharp spotty x-ray diffraction patterns with large variations in the peak intensities and its appearance. This single crystal nature was easily discerned from the broad diffuse features of untransformed CO_2-III and highly disordered carbon. To monitor the phase change during heating, multiple diffraction patterns were obtained *in situ* every 3 to 10 seconds at the center of heating spot, while simultaneously measuring the temperatures by a spectropyrometer. To obtain the spatially resolved structural information of quenched sample, multiple x-ray diffraction data were collected in 5 μm increments across the laser-heated area, with and without small rotations of cells in the Ω direction within ±5°. We used an on-axis dual-beam laser-heating system[24] and, for x-ray diffraction, a focused monochromatic x-ray beam ($\lambda = 0.2907$ Å) and a large-format *a*-Si x-ray array detector (PerkinElmer 1621, 2048 × 2048 pixels) at the Extreme Condition Beamline (P02.2) at the PETRA III.

III. RESULTS

Because of relatively long time (~10 sec or longer) required to obtain angle dispersed powder x-ray diffraction (ADXD), it is difficult to probe the transition in real-time during laser heating. Therefore, in this paper, we focus on discussing the spatially resolved ADXD (SR-ADXD) patterns obtained across the laser-heated area using a small x-ray beam (~2 μm full width at ~50% of intensity). This is important to characterize subtle differences in crystal structures and associated transitions. Figure 1, for example, illustrates the SR-ADXD obtained every 5 μm across the laser-heated carbon dioxide at 49 GPa as shown in the inset: (a) as recorded on the 2*D* x-ray detector and (b) as plotted the integrated intensity scanned as a function of 2θ after removal of the structureless background. The inset in (b) shows a microphotograph of the laser-heated sample and an approximate direction (marked by the white arrow) along which the x-ray diffraction patterns were obtained. The diffraction patterns in (b) are separated by 5 μm approximately along the arrow direction of laser-heated area, whereas the three diffraction images in (a) are selected ones approximately at the center (top) and edge (middle) of laser heated area (appears as the black area) and the outside (bottom).

The SR-ADXD in Fig. 1 indicates the transition of phase III to phase V present in two different polymorphs: (i) tridymitelike phase V_{TD} ($P2_12_12_1$) as evident from the characteristic triplet of (011), (111), and (201) centered at around $2\theta = 5.5°$ and the (103) reflection at 8.6° and (ii) β-crystobalite phase V_{CR} (I-$42d$) as evident from the (101) at 5.5° and (111) at 8.6°. Interestingly, the phase V_{TD} is the major product found at the center of the laser-heated spot, surrounded by the V_{CR} at the edge and unconverted phase III outside the laser-heated area. This result is consistent with that of the earlier laser-heating experiments reporting the V_{TD} by laser heating of phase III at 48 GPa and ~1800 K.[9]

The present result, however, is different from the laser-heating result that showed V_{CR} the only product.[11] Nevertheless, one should keep in mind that the V_{CR} is produced by laser heating a mixture of highly compressed phase II and IV at 39 GPa, which was originally produced at ~21 GPa. In order to evaluate the initial phase dependence of the transition, we have performed the laser-heating experiments of phase II, IV, and III at 39 and 44 GPa as shown in Fig. 2. Similar to the previous study,[11] we were able to produce both phase II and IV at ~24 GPa by laser-heating phase III to relatively low temperatures (below 1000 K). The presence of both phases

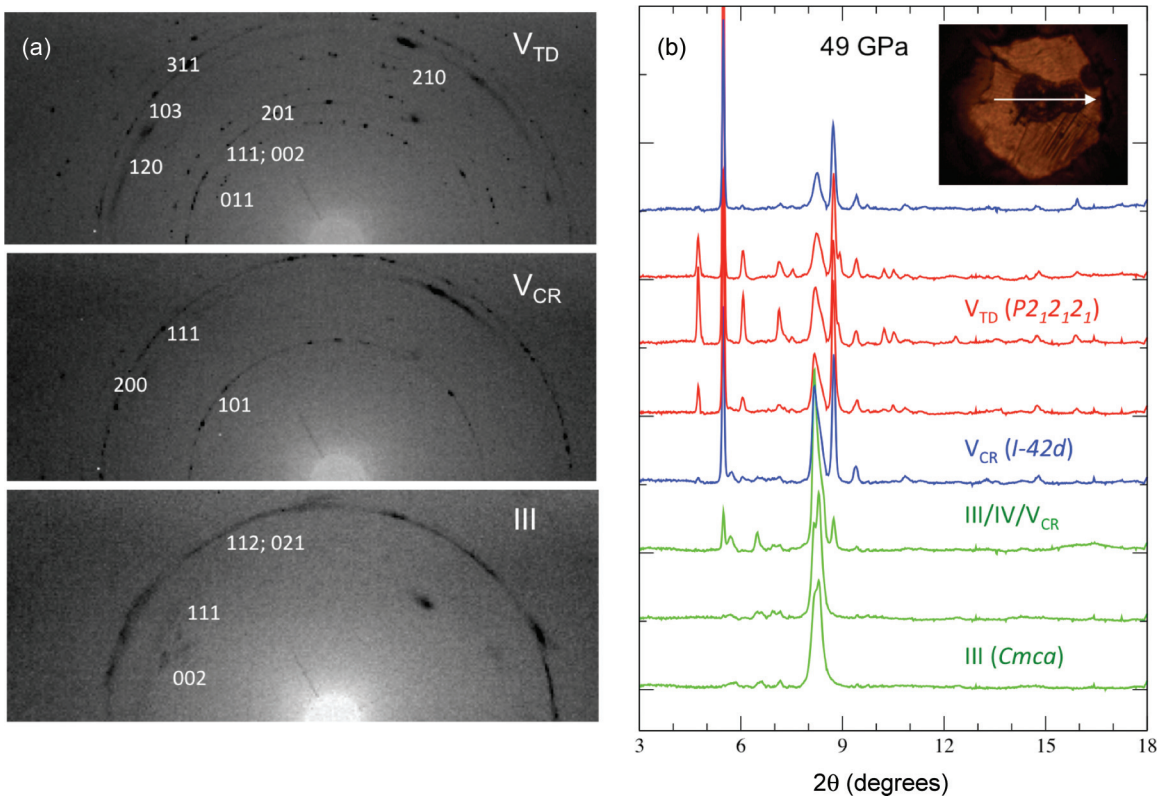

FIG. 1. (Color online) Spatially resolved, angle-dispersed x-ray diffraction (SR-ADXD) patterns obtained across the laser-heated carbon dioxide at 49 GPa as (a) recorded in two-dimensional images and (b) plotted the integrated intensity as a function of 2θ after removing the structureless background. The inset shows a microphotograph of the laser-heated CO_2 sample, together with the x-ray diffraction scan direction along the arrow. The diffraction patterns in (b) are separated by 5 μm approximately along the arrow direction of laser-heated area, whereas three representative diffraction images in (a) are approximately at the center (top) and edge (middle) of laser-heated area (appears as the black area) and the outside (bottom). The SR-ADXD indicates that the transition occurs from phase III (*Cmca*) to V coexisting in two polymorphs: tridymitelike V_{TD} phase ($P2_12_12_1$) at the center of the heating spot and β-cristobalitelike V_{CR} phase (I-42d) at the edge.

was confirmed visually by its annular appearance of highly polycrystalline phase II surrounding transparent phase IV at the center of heated area, as well as their characteristic x-ray diffraction patterns. No extended phase was formed at this pressure. Then, the pressure was increased to 39 GPa and laser heated to transform (a) the phase II to the V_{CR} phase and (b) the phase IV (or II) to the V_{CR}. No evidence for the V_{TD} phase was found at this pressure. Then, we further increased the pressure to 44 GPa and laser heated to transform (c) the phase III to both V_{TD} and V_{CR} phase. Again, the V_{TD} was the major product and the V_{CR} phase was only found at the edge of the heating area. In all cases, the temperature was estimated to be ~1700–1800 K. A little variation in the observed transition temperature confirms the kinetically controlled process as suggested previously.[7,9,11,12] The pressure gradient on the other hand is estimated to be less than 2–3 GPa within the laser-heated area (~30 μm), based on the pressure gradient of phase III at this pressure ~100 GPa/mm. Thus, the difference in the observed transformations cannot be explained in terms of pressure or temperature gradient of the laser-heated area, but underscores the path-dependent nature of carbon dioxide transformations. That is, the phase II and IV transform into the V_{CR} below 40 GPa whereas the phase III transforms into the V_{TD} phase above 40 GPa. Thus, it explains the different observations in the previous laser-heating experiments.[9,11,12]

Note that the diffraction patterns for highly compressed phases II, IV, and III are considerably deformed, as expected at pressures 39–44 GPa.[4,25] As such, it is difficult to make rigorous structural refinements on those phases. Nevertheless, we were able to refine the diffraction patterns reasonably well, especially for phase V_{CR} and V_{TD}, as shown in Fig. 3 and summarized in Table I. The refinement of V_{CR} was quite straightforward for its well-defined atomic positions of carbon at 4a (0,0,0) and oxygen at 8d (x,1/4,1/8). A full-scale Rietveld refinement was performed using the I-42d structure ($Z = 4$) for an appropriate scale factor, zero-shift, lattice parameters, peak profile, u, v, w, and atomic positions with anisotropic temperature factors. Small impurity peaks at 7.1° and 10.1°, coming from unreacted carbon used for the laser heating, were masked during the refinement process. No preferred orientation was included. For the mixed phase data, the phase fraction was also refined. The final results of the refined patterns in Fig. 3(a), for example, yield $a = b = 3.594(1)$ Å, $c = 5.917(2)$ Å, and $\rho = 3.824$ g/cm^3 for phase V_{CR} and $a = b = 3.427(1)$ Å, $c = 4.040(2)$ Å, and $\rho = 3.081$ g/cm^3 for phase II. These results show good agreements in intensity with $R_{wp} = 1.21\%$ $R_p = 0.7\%$, $wR_p = 2.56\%$

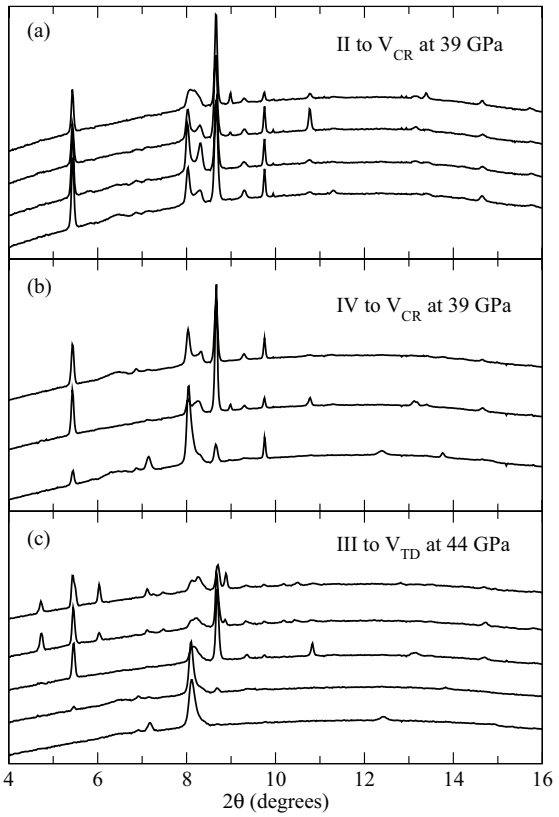

FIG. 2. The SR-ADXD patterns of laser-heated carbon dioxide showing (a) phase II to V_{CR} transition at 39 GPa, (b) phase IV to V_{CR} transition at 39 GPa, and (c) phase III to V_{TD} transition at 44 GPa. The phase II and IV was produced by laser heating the phase III at 25 GPa to relatively low temperatures (<1000 K) and then compressed to 39 and 44 GPa for laser-heating experiments to produce phase V. Also, see Fig. 3 for Rietveld refinements of several selected patterns.

with reduced $\chi^2 = 1.56$. No significant structural difference of phase II either in V_{CR} region [the top pattern in Fig. 3(a)] or in phase II rich region [the bottom in Fig. 3(a)] was observed. The refined crystal structures of phase V_{CR} agree with the previous reports at similar pressures,[11,12] including the C-O distance in CO_4 tetrahedra of 1.373 Å and two C-O-C angles of 137° and 116°. The refined densities of phase II (3.081 g/cm^3) and IV (3.037 g/cm^3) are also well matched with those reported previously.[3,5,9] The refined results for all phases are summarized in Table I.

The structural refinement of phase V_{TD} in comparison was a little bit tricky for several reasons: first, its low symmetry $P2_12_12_1$ structure with a relatively large number of molecules per unit cell, $Z = 8$. Second, all elements occupy the general position of $4a$ (x,y,z) and especially the oxygen atoms are highly disordered. Third, a relatively small number of peaks, many degenerated, observed in the fundamental diffraction region at low 2θ angles for this low-symmetry structure. Because of these reasons, we first used the XRDA program[26] to determine the initial lattice parameters and corresponding Miller indices of the observed peaks, then, the GSAS program[27] to refine lattice parameters and all other structural parameters. The initial positions of carbon and oxygen atoms

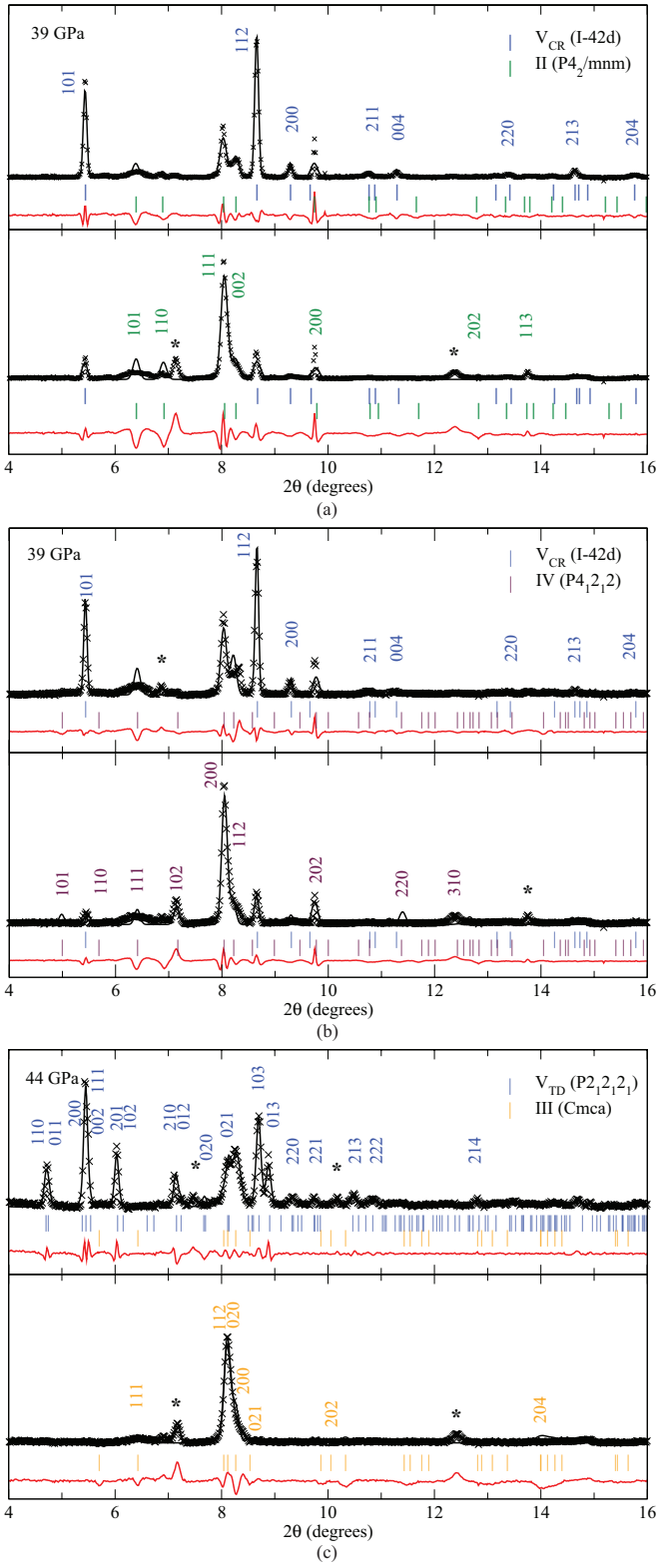

FIG. 3. (Color online) Rietveld refinements of the SR-ADXD patterns of the initial (bottom) and final phases (top) across the phase transitions: (a) from phase II to V_{CR} at 39 GPa, (b) phase IV to V_{CR} at 39 GPa, and (c) phase III to V_{TD} at 40 GPa. These spectra are selected from the top and bottom spectra of Figs. 2(a), 2(b), and 2(c), respectively. The asterisks are features from untransformed phase III not used for the refinement. The final refined crystal structures of each phase are summarized in Table I.

TABLE I. Crystal structures of CO_2 phases at high pressures and ambient temperature.

Phase	V_{CR} at 39 GPa	V_{TD} at 44 GPa	II at 39 GPa	III at 44 GPa	IV at 39 GPa
SG	I-42d	$P2_12_12_1$	$P4_2/mnm$	$Cmca$	$P4_12_12$
Z	4	8	2	4	4
a (Å)	3.594 (1)	6.266 (3)	3.427 (1)	4.027 (7)	4.135 (1)
b (Å)	3.594 (1)	4.386 (2)	3.427 (1)	4.140 (8)	4.135 (1)
c (Å)	5.917 (2)	6.087 (2)	4.040(2)	5.831 (10)	5.629 (2)
V (Å^3)	76.44 (2)	167.29 (8)	47.45 (3)	97.22 (10)	96.26 (6)
ρ (g/cm^3)	3.824	3.495	3.081	3.007	3.037
			Atomic positions		
	C 4a (0 0 0)	C 4a (0.444 0.704 0.164)	C 2a (0 0 0)	C 4a (0 0 0)	C 4a (0.472 0.472 0)
	O 8d (0.213 0.250 0.125)	C 4a (0.062 0.578 0.311)	O 4f (0.755 0.755 0)	O 8f (0 0.716 0.863)	O 8b (0.225 0.206 0.288)
		O 4a (0.491 0.127 0.525)			
		O 4a (0.262 0.527 0.258)			
		O 4a (0.429 0.963 0.232)			
		O 4a (−0.052 0.432 0.163)			

were adopted from the previously reported structure[9] with the individual atomic positions constrained to yielding the C-O distance within 1.2 to 1.6 Å range. This procedure results in the final refined structural parameters of $a = 6.266(3)$, $b = 4.486(2)$, $c = 6.087(2)$ Å, and $\rho = 3.495$ g/cm^3 for the V_{TD} phase and $a = 4.027(7)$, $b = 4.140(8)$, $c = 5.831(10)$ Å, and $\rho = 3.007$ g/cm^3 for the phase III, with $R_{wp} = 1.29\%$ $R_p = 0.8\%$, $wR_p = 3.06\%$ with reduced $\chi^2 = 2.54$. Again, these refined structural parameters are in good agreement with those reported previously.[9]

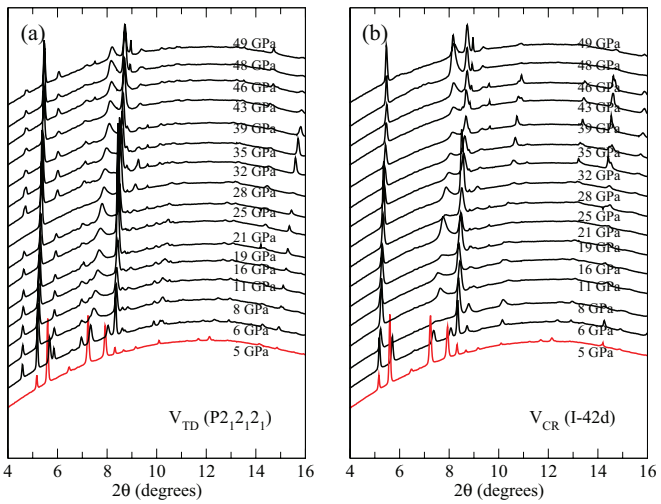

FIG. 4. (Color online) The pressure-dependent SR-ADXD changes of (a) phase V_{TD} and (b) V_{CR} upon unloading pressure from 49 GPa. Note that both polymorphs maintain over a large pressure domain down to 10 GPa, below which they slowly convert into phase I on a time scale of hours.

Figure 4 summarizes the pressure-dependent ADXD changes of (a) phase V_{TD} and (b) V_{CR}, as measured during pressure unloading from 49 GPa. It clearly shows both V_{TD} and V_{CR} polymorphs present well below their stability fields, down to ∼10 GPa. Below 10 GPa, they slowly convert into phase I (Pa-3) in a time scale of hours. Importantly, note that there is no conversion between the V_{TD} and V_{CR} phases, indicating that each polymorphs are locked in their configuration over a large pressure range. As such, there is no easy transformation pathway between the two, once they are formed.

Based on the diffraction data in Fig. 4, we obtained the pressure-volume relationships of the phase V_{TD} (blue solid circles) and V_{CR} (blue open circles), as summarized in Fig. 5. Also plotted together are the previous data of the phase V_{TD} in green open circles from Ref. 9 and the phase V_{CR} from Ref. 11 in red solid triangles for 1% CO_2 in He and red open triangles for pure CO_2. The solid lines are the third-order Birch–Murnaghan equation-of-state fits[28] to each set of the data with the parameters listed in Table II. Clearly, the present results are comparable to the previous ones. Interestingly, the density of phase V_{CR} is substantially higher (∼12% at 50 GPa) than that of the V_{TD}; whereas, the V_{CR} ($B_o\{B\}' = 120\{5.8\} - 135\{3.6\}$ GPa) is considerably softer than the $V_{TD}(270\{1.9\} - 365\{1.0\}$ GPa). This leads to a 4%–5% density difference between the two polymorphs at ambient pressure, which can be compared with the 1%–3% density difference observed between various polymorphs of cristobalite and tridymite in SiO_2.[29] Note, however, that in SiO_2 the polymorphs of tridymite are generally denser than those of cristobalite. Interestingly, theory predicts similarly high bulk moduli for a hexagonal form of tridymite ($P6_3/mmc$, $B_o = 135$ GPa) and for an ideal cubic form of β-cristobalite ($Fd3m$, 129 GPa) that are substantially greater than any other forms of fourfold SiO_2 polymorphs (typically ∼10–40 GPa).[30] Therefore, considering substantially stronger covalent bonds

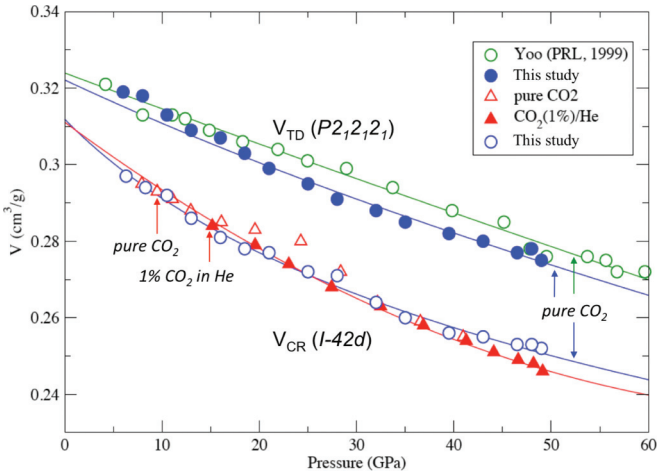

FIG. 5. (Color online) The pressure-volume compression curves of phase V_{TD} (blue solid circles) and V_{CR} (blue open circles), compared with the previous results of phase V_{TD} in Ref. 9 (green open circles) and phase V_{CR} in Ref. 11 (red solid triangles for 1% CO_2 in He and red open triangles for pure CO_2). The solid lines are the third-order Birch–Murnaghan fits to each set of the data using the parameters summarized in Table II. Note that V_{CR} is substantially denser but softer than V_{TR}.

of C-O and thereby the rigidity of CO_4 tetrahedral structures, it is interesting but not a surprise to find such a large difference in the bulk moduli between the V_{TD} and V_{CR} phases. Finally, the present compression data of the V_{CR} shows no sign of lattice distortion observed in the previous V_{CR} data of pure CO_2 at ~15 to 25 GPa and deviates from the previous 1% CO_2 data above 40 GPa.[11] The present density of the V_{TD}, on the other hand, is somewhat higher than the previous one by about 0.5%–1.5% depending on pressure.[9]

IV. DISCUSSION

The present structural models in Table I can explain the observed path (or initial phase) dependence of the phase IV-to-V_{CR} and III-to-V_{TD} transitions and their structural relationships as illustrated in Fig. 6. Note that phase IV is related to phase II by doubling up the unit cell along the c axis. This relation results from a slightly bent molecular configuration of phase IV, which makes it isostructural to α-crystobalite ($P4_12_12$). The phase IV at 39 GPa is compressed to about 12% from that at 20 GPa, which brings the nearest carbon-oxygen distances within ~2.1 Å. Having an additional 25% volume collapse associated with the phase IV-to-V_{CR} transition at

TABLE II. The third-order Birch–Murnaghan equation of state parameters of CO_2-V determined in this study in comparison with those of the previous reported.

CO_2-V	B (GPa)	B_0'	V_0/Z
Yoo (PRL, 1999)	326.7	1.0	23.7
Tridymite (this paper)	267.5	1.5	23.7
Cristobalite (this paper)	126.4	6.6	22.7
Datchi (PRL, 2012)[a]	136.0	3.6	22.8

[a]The EOS values are of a highly diluted sample of 1% CO_2 in He.

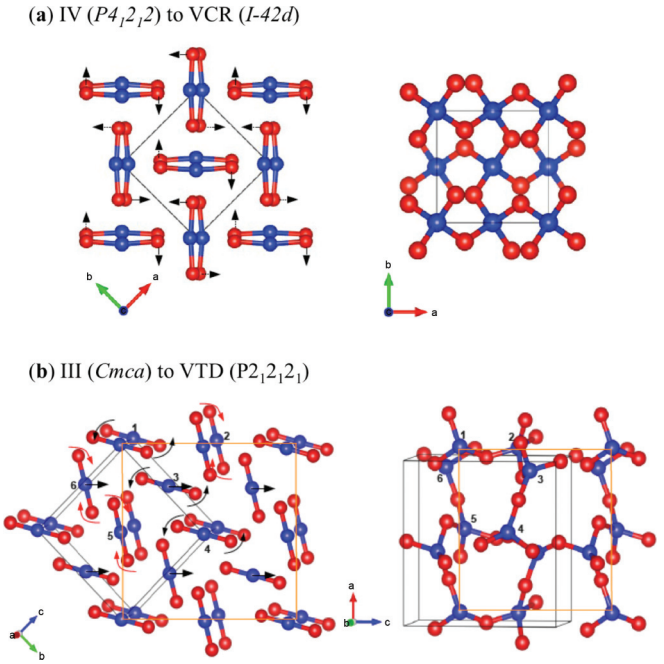

FIG. 6. (Color online) Structural relationships of carbon dioxide phases governing (a) the phase IV to V_{CR} transition, which occurs displacively by simple rotation and bending of CO_2 molecules without significant movement of carbon atoms and (b) the phase III to V_{TD} transition, occurring diffusively by both translation of carbon atoms and rotation of O-C-O bonds. The straight and arc arrows signify the translation and rotation of atoms, while the black and red arrows represent the motions within and out of the plane, respectively. The grey and orange boxes represent the unit and $(1 * \sqrt{2} * \sqrt{2})$ super cells of different phases. The numbers signify six carbon atoms in phase III, transforming to six corner shared CO_4 tetrahedra in phase V_{TD}.

39 GPa,[11] the structure of phase IV would become nearly extended with the nearest C-O distance of ~1.9 Å—very much like α-crystobalite in SiO_2. Then, the transition from this α-cristobalitelike phase IV to the β-crystobalitelike V_{CR} can take place simply by slightly rotating CO_2 molecules within the ab plane [as illustrated in Fig. 6(a)] without movement of carbon atoms—the process involving a small kinetic barrier. In fact, it is well known that the α- to β-cristobalite transition in SiO_2 does occur, displacively and discontinuously, by simply tilting the corner-sharing SiO_4 tetrahedral in distorted sixfold holohedral rings.[31] This process is equivalent to the rotation of corner-shared oxygen atoms in O-Si-O.

In contrast to the displacive IV (or II)-to-V_{CR} transition within a direct group-subgroup relationship, the III-to-V_{TD} transition involves diffusive motions of carbon and oxygen atoms as illustrated in Fig. 6(b). Note that both phase III ($Cmca$) and phase V_{TD} ($P2_12_12_1$) have similar layer structures along the a and c axes, respectively. Furthermore, because the b and c axes of phase III and the a and c axes of phase V_{TD} are different only by ~2.1% and ~3.3%, respectively (see Table I), the crystal structure of phase III and V_{TD} can be considered as a distorted tetragonal structure. Therefore, a supercell of phase III with eight CO_2 (the $1 * \sqrt{2} * \sqrt{2}$ cell marked in orange lines) can be related to a unit cell of phase V_{TD} by permuting the stacking a axis of phase III and c axis of phase

V_{TD}. Then, the III-to-V_{TD} transition can be recognized by two transformations: (i) the translation of eight face-centered CO_2 molecules by ~1/4 unit cell distance along the c_{III}' axis (marked in black straight arrows) and (ii) the counteracting rotation of oxygen atoms, the half (connected to C1, C3, and C4) within the $b'c'$ plane (black arc arrows) and the other half (C2, C5, and C6) out of the plane (red arc arrows). These transformations then result in six CO_2 molecules forming a buckled 12-member ring, or six corner-shared CO_4 tetrahedra (C1 through C6) of phase V_{TD}, where C1 and C2 in the first layer, C3 and C6 in the second layer, and C4 and C5 in third layer are corresponding to the 2_1 glide planes in screw a axis.

In the V_{TD} structure, the CO_4 tetrahedral units share their corner oxygen atoms to form sixfold distorted holohedral rings with alternating tetrahedral apices pointing up and down the ab plane. The apices of tetrahedra are then connected through oxygen atoms along the c axis. This open structure of the V_{TD} is contrary to the partially collapsed structure of the V_{CR}, in which CO_4 polyhedra are tilted by ~38° along the c axis.[12] As such, the V_{CR} is substantially denser than the V_{TD}, and the transition between the V_{CR} and V_{TD} phases is strongly forbidden without significant diffusion of atoms and defects. This is likely the reason why the V_{CR} is observed only at the interfacial area between the V_{TD} and untransformed phase III and why the V_{TD} is absent below 40 GPa [in Figs. 3(a) and 3(b)]. In addition, the V_{CR}-to-V_{TD} transition is energetically forbidden below 40 GPa, so is the III-to-V_{TD} transition with respect to the III-to-II (or IV) between 20–40 GPa. Note that phase III is unstable with respect to phase II in this pressure range,[32] but it exists only because the I-to-III transition involves a relatively small kinetic barrier at ambient temperature with respect to the I-to-II transition.

First principles calculations[8,10] suggest that β-cristobalite is most stable of all fourfold extended carbon dioxide phases including α- and β-quartz, m-chalcopyrite, tridymite, and coesite. Nevertheless, the energy difference of these polymorphs is relatively small with respect to the compression energy ($P\Delta V$) that drives the molecular-to-nonmolecular transition. For example, the enthalpy difference between β-cristobalitelike V_{CR} phase and tridymitelike V_{TD} phase is less than 0.3 eV/CO_2—sufficient to differentiate the ground state in first principles calculations, but too small to prevent other reaction pathways during laser-heating experiments. Note that the enthalpy difference between phase III and V_{TD} at 50 GPa is, for example, over 1 eV/CO_2.[33] Therefore, it is plausible that this large disparity in energy leads to overcoming the associated diffusion barrier in the III-to-V_{TD} transition and the observed large distortion in the V_{TD} structure. On the other hand, the above-mentioned structural relationship controls the specific transition to occur via the transition pathway involving a lower activation barrier; that is, either displacively from phase IV (or II) to phase V_{CR} or diffusively from phase III to phase V_{TD}—despite the large density difference between the two polymorphs.

The present results also provide new constraints regarding the stability field of phase V. First, phase V_{TD} arises from compressed phase III above 40 GPa, whereas phase V_{CR} from compressed phase IV (or II) below 40 GPa. Second, the large density difference between V_{TD} and V_{CR} indicates the negative slope in $\Delta T/\Delta P$ for the V_{TD}-V_{CR} phase boundary. Third,

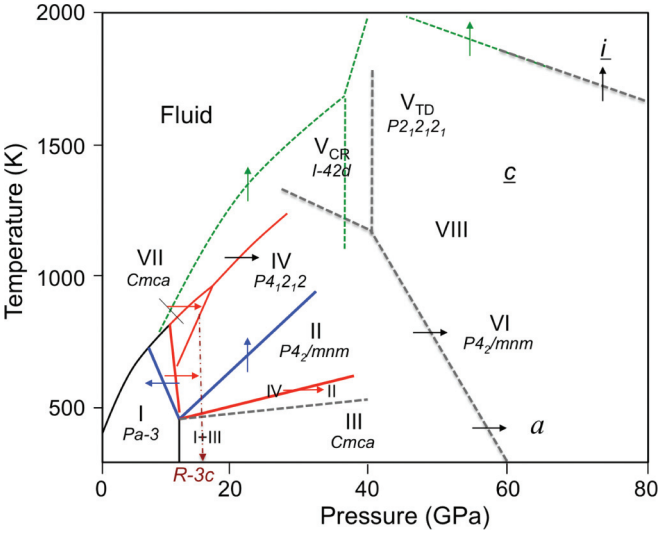

FIG. 7. (Color online) Phase and chemical transformation diagram of carbon dioxide, exhibiting a wide range of silicatelike nonmolecular phases. The letters a, c, and i represent amorphous-CO_2 (a-carbonia), coesitelike CO_2 (c-CO_2), and extended ionic CO_2 (i-CO_2). Arrows signify the thermal pathways measured each phase boundaries, reported in Ref. 2 in red solid lines, Ref. 19 in green dotted lines, Refs. 13 and 25 in blue solid lines, and Ref. 18 in black dotted lines. The c notes the path-dependent nature of c-CO_2, produced by laser heating of quenched phase VI.[15] Strongly path-dependent phase IV and II boundaries underscore the intermediary nature of these phases. The R-3c structure was observed from the quenched single crystal phase IV at ambient temperature and 15 GPa, which was originally grown in the stability field of phase VII at 11.7 GPa and 830 K.[34]

the phase V_{CR} can be formed from phase IV at pressures as low as 20 GPa in a presence of catalysts.[30] Finally, the phase V_{CR} can be produced at substantially lower temperatures than the V_{TD} (typically above ~1700–1800 K). This is also consistent with the fact that the V_{TD} was observed at the center of heating spot (i.e. the hottest area), surrounded by the V_{CR} in Fig. 1. Nevertheless, it is important to realize that the measured transition temperature during laser heating is not a good parameter, because it represents the temperature of heat absorber not CO_2 itself. In this regard, it is the upper bound of the transition temperature. On the other hand, the endothermic nature of the molecular-to-nonmolecular transition brings the measured temperature to the lower bound.

Based on the above-mentioned constraints together with those of the previous studies,[1,2,18,19,34] one can construct the phase and chemical transformation diagram of carbon dioxide as shown in Fig. 7. Early high-pressure studies have established the existence of two molecular solid phases of CO_2: cubic ($Pa3$) phase I and orthorhombic ($Cmca$) phase III, both stabilized by quadrupolar interactions between linear molecules.[1] Recent studies have found another molecular phase VII ($Cmca$) at high temperatures near the melt and the phase I stability field.[2] Above 40–60 GPa, these molecular solids transform into a wide range of nonmolecular extended phases, which include tetrahedral bonded polymeric V_{CR} and V_{TD}, disordered sixfold phase VI, coesitelike c-CO_2, and silicalike amorphous CO_2 (a-carbonia). Between the stability

fields of molecular and extended phases at pressures of 20 to 40 GPa, there are unusual intermediary phases IV and II, of which stability fields depend strongly on the thermal pathways of measurements, as signified in Fig. 7 by the arrows on the phase boundaries for the measured thermal directions. In turn, such strong path-dependences observed on the phase IV and II boundaries underscore the presence of relatively strong intermolecular interactions (or intermediate bonding) in these phases.

It should also be mentioned that the R-3c structure was observed from the quenched single-crystal phase IV at ambient temperature and 15 GPa.[34] However, in this study the single-crystal phase IV was initially grown near the phase IV-VII-liquid triple point (11.7 GPa and 830 K), then annealed the sample at 15 GPa and 830 K and quenched to ambient temperature at 15.2 GPa. Note that the 11.7 GPa is well within the molecular regime near the stability field of phase I—far from the pressure regime where phase IV develops strong intermolecular bonding (typically ∼20 GPa). Therefore, it is plausible that the quenched phase in R-3c represents either disordered or, more likely, an expanded form of intermediate phase IV, as observed a similar disorder or a compressed form upon elevating pressure (see Fig. 6). In fact, the R-3c structure is very similar to the P-3a structure of phase I, both commonly observed in typical molecular solids such as N_2 and CO.[35]

While the phase boundaries of extended phases are not well understood, the phase and chemical transformation diagram in Fig. 7 reveals the analogy (or difference) between CO_2 and SiO_2. For example, it is like SiO_2 that the phase IV-to-V_{CR} transition occurs highly discontinuously and the β-cristobalitelike V_{CR} phase appears at higher temperatures than the α-cristobalitelike phase IV. However, unlike SiO_2, the V_{TD} appears at higher pressures than the V_{CR}, and there is no quartzlike fourfold structure found in CO_2. It is also unlike SiO_2 that at high temperatures all extended phases further transform into carbon dioxide carbonate (i-CO_2)[18]—a fully extended 2D ionic layer structure of the post aragonite of $CaCO_3$ ($P2_12_12$).[36] Note that this $P2_12_12$ structure of $i-CO_2$ is in a sub/supergroup relation with the $P2_12_12_1$ of V_{TD} and $P4_12_12$ of α-cristobalite and is similar to the layer structure theoretically predicted earlier.[8] On the other hand, another laser-heating study[19] reports the decomposition of CO_2 phases to carbon and oxygen at the onset of the ionization line in Fig. 7. This difference, again, displays the significance of chemical kinetics associated with the ionization and decomposition processes, which depend on factors such as how long the phase has been annealed at a particular temperature and pressure.[37] In this regard, the stabilities of many extended phases including a-CO_3, phase VI, VIII, and i-CO_3 are not well understood, so are their phase boundaries.

In conclusion, this paper confirmed the presence and properties of both V_{TD} and V_{CR} phases, as reported previously.[9,11,12] This includes substantially higher bulk modulus and lower density of the V_{TD} than those of the V_{CR}. The transitions to these phases depend on the initial phases and occur either diffusively from phase III to V_{TD} or displacively from phase IV to V_{CR}. We also presented the phase/chemical transformation diagram of carbon dioxide, exhibiting the path-dependent nature of transitions especially to/from phase II and IV, which in turn signifies the intermediary nature of these phases. In this regard, highly compressed form of phase IV (above 40 GPa) should be considered as extended α-cristobalite ($P4_12_12$), whereas its expanded form (below 20 GPa) as a molecular solid (R-3c).

ACKNOWLEDGMENTS

The x-ray diffraction experiments were performed on the Extreme Conditions Beamline (P02.2) of PETRA III in DESY, a member of the Helmholtz Association. This paper has been supported by NSF-DMR (Grant No. 1203834), DTRA (HDTRA1-12-01-0020) and Deep Carbon Observatory—Extreme Physics and Chemistry.

*Corresponding author: csyoo@wsu.edu

[1] K. Aoki, H. Yamawaki, M. Sakashita, Y. Gotoh, and K. Takemura, Science **263**, 356 (1994).
[2] V. M. Giordano and F. Datchi, Europhys. Lett. **77**, 46002 (2007).
[3] C. S. Yoo, H. Kohlmann, H. Cynn, M. F. Nicol, V. Iota, and T. LeBihan, Phys. Rev. B **65**, 104103 (2002).
[4] C. S. Yoo, V. Iota, and H. Cynn, Phys. Rev. Lett. **86**, 444 (2001).
[5] J. H. Park, C. S. Yoo, V. Iota, H. Cynn, M. F. Nicol, and T. Le Bihan, Phys. Rev. B **68**, 014107 (2003).
[6] F. A. Gorelli, V. M. Giordano, P. R. Salvi, and R. Bini, Phys. Rev. Lett. **93**, 205503 (2004).
[7] V. Iota, C. S. Yoo, and H. Cynn, Science **283**, 1510 (1999).
[8] S. Sera, C. Corazon, G. L. Chiarotti, S. Scandolo, and E. Tossatti, Science **284**, 788 (1999).
[9] C. S. Yoo, H. Cynn, F. Gygi, G. Galli, M. Nicol, D. Hausermann, S. Carlson, and C. Mailhiot, Phys. Rev. Lett. **83**, 5527 (1999).
[10] J. Dong, J. K. Tomfohr, O. F. Sankey, K. Leinenweber, M. Somayazulu, and P. F. McMillan, Phys. Rev. B **62**, 14685 (2000).
[11] F. Datchi, B. Mallick, A. Salamat, and S. Ninet, Phys. Rev. Lett. **108**, 125701 (2012).
[12] M. Santoro, F. A. Gorelli, R. Bini, J. Haines, O. Combon, C. Levelut, J. A. Montoya, and S. Scandolo, Proc. Natl. Acad. Sci. **109**, 5176 (2012).
[13] Valentin Iota, C. S. Yoo, J. Klepeis, Jeni Zsolt, W. Evans, and H. Cynn, Nat. Mater. **6**, 34 (2007).
[14] J. Sun, D. D. Klug, R. Mortonak, J. A. Montoya, M. S. Lee, S. Scandolo, and E. Tosatti, Proc. Natl. Acad. Sci. **106**, 6077 (2009).
[15] A. Sengupta and C. S. Yoo, Phys. Rev. B **82**, 012105 (2010).
[16] M. Santoro, F. A. Gorelli, R. Bini, G. Ruocco, S. Scandolo, and W. A. Crichton, Nature **441**, 857 (2006).
[17] J. A. Montoya, R. Rousseau, M. Santoro, F. Gorelli, and S. Scandolo, Phys. Rev. Lett. **100**, 163002 (2008).
[18] C. S. Yoo, A. Sengupta, and M. Kim, Angew. Chem., Int. Ed. **50**, 11219 (2011).
[19] K. D. Litasov, A. F. Goncharov, and R. J. Hemley, Earth Planet. Sci. Lett. **309**, 318 (2011).

[20]B. Holm, R. Ahuja, A. Belonoshko, and B. Johansson, Phys. Rev. Lett. **85**, 1258 (2000).
[21]E. Gregoryanz, A. F. Goncharov, R. J. Hemley, and H. K. Mao, Phys. Rev. B **66**, 224108 (2002).
[22]M. Hanfland, R. J. Hemley, H. K. Mao, and G. P. Williams, Phys. Rev. Lett. **69**, 1129 (1992).
[23]J. Yen and M. Nicol, J. Appl. Phys. **72**, 5535 (1992).
[24]Z. Konopkova, H. P. Liermann, and W. Morgenroth, *Photon Science 2012: Highlights and Annual Report* (Deutsches Elektronen-Synchrotron DESY, Hamburg, 2012), p. 110.
[25]C. S. Yoo, A. Sengupta, and M. Kim, High Pres. Res. **31**, 68 (2011).
[26]S. Desgreniers and K. Lagarec, J. Appl. Crystallogr. **31**, 109 (1998).
[27]A. C. Larson and R. B. Von Dreele, Los Alamos National Laboratory Report LAUR 86-748 (2000).
[28]F. Birch, Phys. Rev. **71**, 809 (1947).
[29]A. K. A. Pryde and M. T. Dove, Phys. Chem. Miner. **26**, 171 (1998).
[30]Th. Demuth, Y. Jeanvoine, J. Hafner, and J. G. Angyan, J. Phys.: Condens. Matter **11**, 3833 (1999).
[31]D. M. Hatch and S. Gibose, Phys. Chem. Miner. **17**, 554 (1991).
[32]S. A. Bonev, F. Gygi, T. Ogitsu, and G. Galli, Phys. Rev. Lett. **91**, 065501 (2003).
[33]A. Sengupta, M. Kim, C. S. Yoo, and John S. Tse, J. Phys. Chem. C **116**, 2061 (2012).
[34]F. Datchi, V. M. Giordano, P. Munsch, and A. M. Saitta, Phys. Rev. Lett. **103**, 185701 (2009).
[35]R. L. Mills, B. Olinger, and D. T. Cromer, J. Chem. Phys. **84**, 2837 (1986).
[36]S. Ono, T. Kikegawa, Y. Ohishi, and J. Tsuchiya, Am. Mineral. **90**, 667 (2005).
[37]C. S. Yoo, Phys. Chem. Chem. Phys. **15**, 7949 (2013).